

# High energy $\gamma$ -ray production from Be, C, and Al targets with 65 MeV $^3\text{He}$ bombardment

著者	石井 慶造
journal or publication title	Physical review. C
volume	54
number	5
page range	2429-2434
year	1996
URL	<a href="http://hdl.handle.net/10097/35229">http://hdl.handle.net/10097/35229</a>

doi: 10.1103/PhysRevC.54.2429

## High energy $\gamma$ -ray production from Be, C, and Al targets with 65 MeV $^3\text{He}$ bombardment

M. Hosaka,\* K. Ishii,<sup>†</sup> M. Ohura, A. Terakawa, S. Miyamoto, Z. Guan, and H. Orihara  
*Cyclotron and Radioisotope Center, Tohoku University, Sendai 980-77, Japan*

J. Kasagi

*Laboratory of Nuclear Science, Tohoku University, Mikamine 1-2-1, Sendai 982, Japan*

(Received 16 May 1995)

High-energy  $\gamma$  rays from targets of Be, C, and Al bombarded with 65 MeV  $^3\text{He}$  ions have been measured by the use of a  $\gamma$ -ray detector system consisting of seven  $\text{BaF}_2$  scintillators. The energy spectra were obtained up to the maximum energy kinematically permitted in each collision at detection angles of  $35^\circ$ – $144^\circ$ . The experimental cross sections are compared with calculations of the potential bremsstrahlung on which the theory has been developed by Nakayama and Bertsch. It is shown that the prediction of potential bremsstrahlung can well reproduce the production cross sections of  $\gamma$  rays of energy near the kinematical maximum energy in collisions, while this result is contrary to the previous one of Tam *et al.* in  $\alpha$  and  $d$  bombardments. [S0556-2813(96)01611-1]

PACS number(s): 23.20.-g, 25.55.-e, 29.30.Kv

### I. INTRODUCTION

Since the late 1980s, high-energy  $\gamma$ -ray productions in nuclear collisions have attracted attention and have been well studied both experimentally and theoretically [1,2]. Characteristics of the energy spectra and angular distributions of  $\gamma$  rays of an intermediate energy  $20 < E < 100$  MeV, emitted during heavy-ion collisions, have been well explained with a model assuming that nucleon-nucleon bremsstrahlung is the main radiative process. In the model, the production of nucleon-nucleon bremsstrahlung beyond half the beam energy per nucleon can be realized by considering the Fermi momentum distribution of nucleons in projectile and/or target nuclei, and change of the phase space during the collision. Cassing *et al.* [3] performed such calculations in which nucleon-nucleon collisions during the reaction are treated by using the transport equation of Boltzmann-Uehling-Uhlenbeck. However, this theory cannot be applied to the production of  $\gamma$  rays near the maximum energy kinematically permitted in collision, because the total energy of the system is not conserved. Nakayama and Bertsch proposed the potential bremsstrahlung [4,5], where the projectile nucleus is assumed as a structureless particle, and  $\gamma$  rays are produced when the projectile is strongly accelerated in the surface of target nucleus.

Although there has been a large amount of experimental work on the production of high-energy  $\gamma$  rays in intermediate heavy-ion collisions, reports on observation of  $\gamma$  rays near the kinematical maximum energy are very few. In the case of a projectile consisting of many nucleons such as nuclei with  $A > 10$ , the potential bremsstrahlung is unlikely to occur since it is difficult to regard the projectile as a structureless particle, while in the case of light ion projectiles such as  $d$ ,

$^3\text{He}$ , and  $\alpha$ , one can expect to observe the potential bremsstrahlung. Nakayama and Bertsch, using an infinite nuclear matter approximation, evaluated the potential bremsstrahlung cross sections and compared with the experimental  $\gamma$ -ray spectra [6] from 27 MeV  $^4\text{He}$ - and  $^3\text{He}$ -induced reactions on a samarium target. Their calculated results poorly reproduce the energy dependence of the  $\gamma$ -ray spectra, and the authors concluded that neither potential field nor nucleon-nucleon collisions can account for measured high-energy tail. However, the reactions analyzed by Nakayama and Bertsch are not appropriate to the test of the potential bremsstrahlung, since the contribution of decay  $\gamma$  rays from the giant dipole resonances of the compound nuclei is considerable in the  $\gamma$ -ray spectra rather than the potential bremsstrahlung. Actually, Reffo *et al.* [7] calculated the contribution of  $\gamma$  rays from the giant dipole resonance excited in a pre-equilibrium relaxation process, and showed a good agreement with the experimental results. The potential bremsstrahlung should therefore be sought for in the  $\gamma$ -ray spectra observed at a projectile energy sufficiently high to avoid the contribution of giant dipole resonance. In this paper, we report on such measurements; energy spectra and angular distributions of high-energy  $\gamma$  rays emitted in the  $^3\text{He}$ -induced reactions at 65 MeV. We have used  $\text{BaF}_2$  scintillators to measure high-energy  $\gamma$  rays, because of its excellent timing property [8] and ability of  $n$ - $\gamma$  discrimination through the pulse shape analysis [9]; these properties play an essential role to reject neutron events in continuum  $\gamma$ -ray spectra. The observed  $\gamma$  rays near the kinematical maximum energy are discussed on the basis of the theory of potential bremsstrahlung.

### II. EXPERIMENT

The experiment of high-energy  $\gamma$ -ray production was performed with 65 MeV  $^3\text{He}$  beams from the AVF cyclotron at Cyclotron and Radioisotope Center, Tohoku University. Natural self-supporting foils of Be, C, and Al with thickness of 18.5, 11.3, and 27.0  $\text{mg}/\text{cm}^2$ , respectively, were bom-

\*Present address: UVSOR, Institute of Molecular Science, Myodaiji, Okazaki 444, Japan.

<sup>†</sup>Present address: Department of Quantum Science and Energy Engineering, Tohoku Univ., Sendai 980-77, Japan.

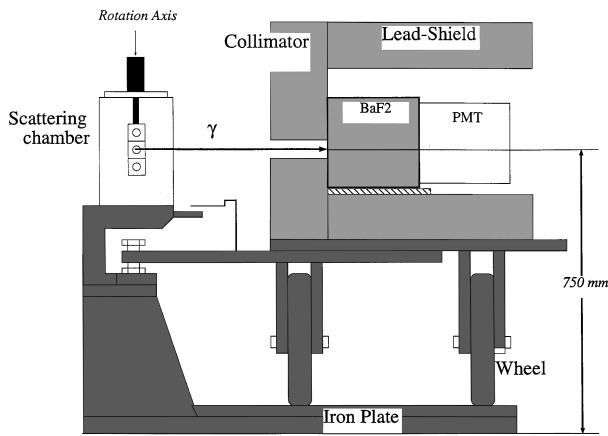


FIG. 1. Layout of high-energy  $\gamma$ -ray measurement system.

barded and  $\gamma$  rays were measured with a high-energy  $\gamma$ -ray detection system. As shown in Fig. 1, the detector was shielded with lead blocks of 10 cm in thickness and mounted on a turntable which can rotate around the target in a plane containing the beam axis from  $35^\circ$  to  $144^\circ$ . The solid angle of high-energy  $\gamma$ -ray detector was defined to be 7.85 msr with a lead collimator of 15 cm in length. Measurements were performed at angles of  $35^\circ$ ,  $60^\circ$ ,  $90^\circ$ ,  $120^\circ$ , and  $144^\circ$  for Be target and at  $35^\circ$ ,  $60^\circ$ ,  $75^\circ$ ,  $90^\circ$ ,  $105^\circ$ ,  $120^\circ$ , and  $144^\circ$  for C and Al targets.

Figure 2 shows the high-energy  $\gamma$ -ray detection system which consists of seven BaF<sub>2</sub> crystals, being optically separated from each other. Each crystal has a hexagonal cross section with a length of the side of 3.75 cm and an axial length of 20 cm. Through a thick collimator,  $\gamma$  rays can hit the central BaF<sub>2</sub> crystal only, and part of its energy may escape as scattered Compton  $\gamma$  rays or electron bremsstrahlung. The escape radiations from the central crystal are measured with the surrounding six crystals. Thus the total energy of a high-energy  $\gamma$  ray is obtained by summing up signals from the central and surrounding detectors. The energy resolution (FWHM) is about 9% in the energy range from 25 to 76 MeV. The detector responses for high-energy  $\gamma$  rays were measured, separately, by using a tagged photon facility [10] of LNS, Tohoku University and are shown in Fig. 3. In the measurement, the on-line calibration of the energy scale was made with 15.1 MeV  $\gamma$  rays from the excited state of  $^{12}\text{C}^*$  ( $15.1\text{ MeV}$ ,  $T=1$ ,  $J^\pi=1^+$ ). A broad peak corresponding to the energy deposited in a BaF<sub>2</sub> crystal by cosmic muons were also used for a high-energy calibration point. In order to monitor both the gain shifts of the electronics and the

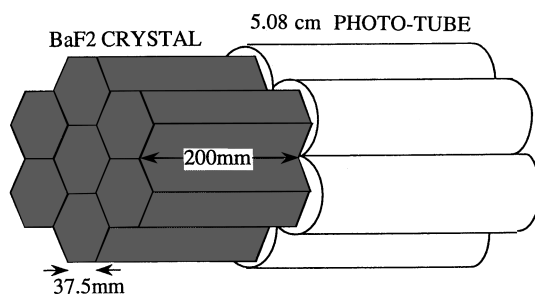


FIG. 2. Construction of the high-energy  $\gamma$ -ray detector.

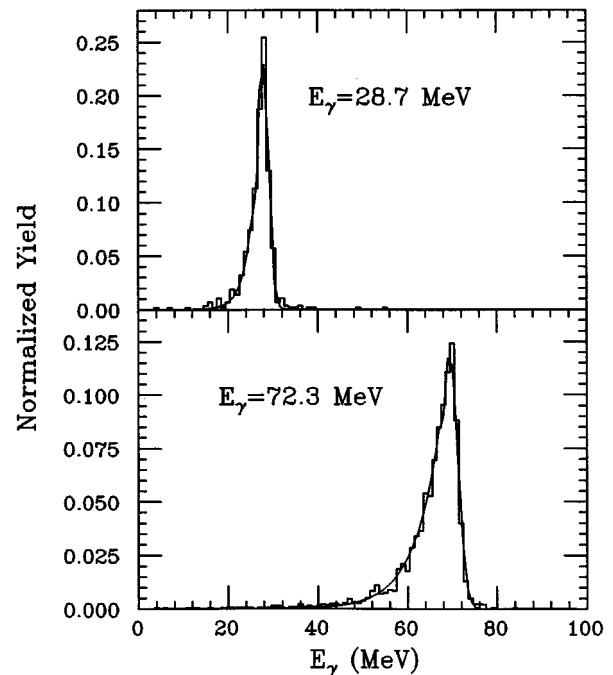


FIG. 3. Response functions for  $\gamma$  rays of 28.7 and 72.3 MeV. Solid curves are the calculations based on Eq. (6).

pileups during the experiment, used was a light emitting diode from which the light was fed into the BaF<sub>2</sub> crystal through optical fibers. Signals of neutrons produced by nuclear reactions were reduced by placing a paraffin block in front of the detector. Remaining neutrons were eliminated by using a time-of-flight technique; the accelerator rf signal and the detector pulse were used as the start and stop signal, respectively. Figure 4 shows a TOF spectrum obtained with a 0.5 m flight path. The time resolution (FWHM) of the  $\gamma$ -ray peak is 1.0–1.5 nsec which is mainly due to the beam time structure. The resolution was small enough to separate  $\gamma$  rays from neutrons in case of the C and Al targets. In the case of the Be target, however, not only this separation technique but also the  $n$ - $\gamma$  discrimination was needed because of a large amount of neutrons. Cosmic-ray backgrounds were

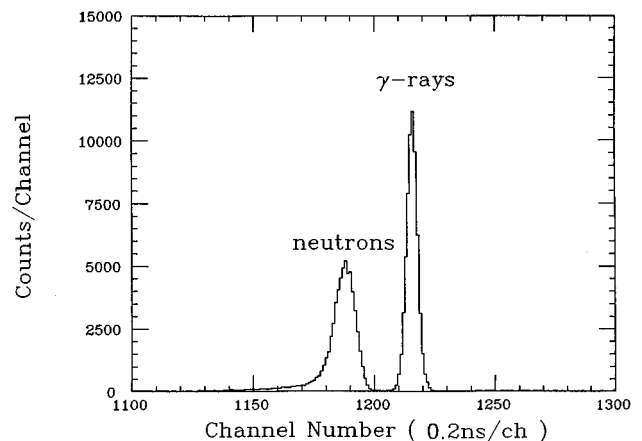


FIG. 4.  $n$ - $\gamma$  discrimination by the T-O-F technique.

eliminated by discriminating the events whose energy is higher than 10 MeV in the surrounding BaF<sub>2</sub> crystals. A reduction factor of 1/20 000 for the cosmic-ray background could be achieved by this discrimination combined with the time-of-flight one. However, it cost the valid  $\gamma$ -ray events; for instance, 11% of the valid events of  $\gamma$  rays at 76.5 MeV were eliminated.

Figure 5 shows energy spectra of high-energy  $\gamma$  rays obtained at laboratory angles of 35°, 90°, and 144°. As shown,  $\gamma$ -ray events are distributed continuously up to the kinematical maximum energy, and sharp  $\gamma$ -ray peaks are not observed except for the C target case, where the 15.1 MeV transition is clearly seen. The spectra indicate that the  $\gamma$  rays were emitted neither isotropic nor symmetric about 90°. The observed asymmetry is remarkable especially for  $E_\gamma \geq 40$  MeV, and should be interpreted as the Doppler shift of radiations in the projectile frame. Since the  $\gamma$ -ray yields in the lower-energy region are expected to contain  $\gamma$  rays decaying from the giant dipole resonance, our discussion in this paper is mainly focused on the production of  $\gamma$  rays of the energy above 40 MeV.

### III. THEORY

The one-dimensional formula [4,5] for the probability of potential bremsstrahlung per unit solid angle and unit photon energy is expressed by

$$\frac{d^2P}{d\omega d\Omega} = z_p^2 \frac{\alpha\omega M_p}{(2\pi)^2 P_i P_f} \times \sum_{\epsilon_k} \left| \int dx e^{ik_x x} \overline{\psi_i(x)} \frac{\epsilon_k \cdot \mathbf{P}}{M_p} \psi_f(x) \right|^2. \quad (1)$$

Here  $\alpha (= 1/137)$  is the fine-structure constant and  $\omega$ ,  $\epsilon_k$ , and  $k_x$  are the energy, the unit polarization vector, and the  $x$  component of the momentum of the photon, respectively.  $M_p$  and  $Z_p$  denote the mass and the atomic number of the projectile.  $P_i$  is the initial momentum before crossing the nuclear surface and  $P_f$  is the final momentum after crossing it.  $\psi_i$  and  $\psi_f$  are the initial and final wave function of the projectile in the Woods-Saxon potential, which is given by

$$V(x) = \frac{V_0}{[1 + \exp(-x/a)]}. \quad (2)$$

Here,  $V_0$  ( $< 0$ ) and  $a$  are the depth and diffuseness of the potential. We consider the production of high-energy  $\gamma$  rays near the kinematical maximum energy, namely, the end point of the bremsstrahlung spectrum. In such a drastic process, the projectile nucleus might receive the nuclear force stronger than in the case of elastic scattering. Thus, we treat  $V_0$  as a parameter, the value of which is not necessarily same as that determined from the elastic scattering data, while the radius of nucleus and the diffuseness  $a$  are geometrical parameters and they should not depend on collision processes (i.e., potential bremsstrahlung and elastic scattering). We use the values of  $a$  obtained from the numerous elastic scattering data of <sup>3</sup>He bombardments. Because of small atomic number of the target nuclei Be, C, and Al, the Coulomb distortion of

$\psi_i$  and  $\psi_f$  is not considered in the present calculation, although it is needed especially in the case of heavier target nuclei.

The differential cross section for the potential bremsstrahlung is obtained by integrating over the impact parameter  $b$  and the azimuthal angle of projectile  $\phi$  in consideration of the spherical geometry of the nuclear surface of target:

$$\frac{d^2\sigma}{d\omega d\Omega} = \int_0^R b db \int_0^{2\pi} d\phi \frac{d^2P}{d\omega d\Omega}, \quad (3)$$

where the initial momentum  $P_i$  in Eq. (1) is adopted as the normal line component  $P_\perp$  of the momentum on the nuclear surface. It is required that the projectile in the final state keeps the same internal structure as that of the initial state. Thus the effective  $Q$  value for the potential bremsstrahlung is expected to be smaller than the actual  $Q$  value of the reaction and to be related to the cluster structure consisting of projectile and target nucleus. We designate this effective  $Q$  value by  $S$  and treat it as a parameter in the present theory. For a given  $P_\perp$ , the maximum available energy to the potential bremsstrahlung is given by

$$\omega_{\max} = \frac{P_\perp^2}{2M_p} + S. \quad (4)$$

The formulation discussed above does not include the contribution of the target. If the target nucleus can be regarded as a point charge, then it can emit a photon also. As the simplest potential model assumes for both the projectile and the target nuclei to be point charges, the correction due to the spatial extent of the charge should be made. Usually, the following factor is used for the correction:

$$\left( F_p(k) - \frac{A_p Z_t}{Z_p A_t} F_T(k) \right)^2, \quad (5)$$

where  $A_t$  and  $Z_t$  stand for the total nucleon number and the atomic number of the target nucleus and  $F_p(k)$  and  $F_T(k)$  are form factors, respectively, for charge density of the projectile and the target nucleus. If  $F(k) = 1.0$ , the nucleus can be regarded as just a cluster of nucleons which behaves as a point charge for a given momentum transfer. Since the observed maximum  $\gamma$ -ray energy in the present work is about 60 MeV, one can assume  $F(k) = 1.0$ ; the spatial extent can be neglected for such a small momentum transfer. Nakayama and Bertsch assumed  $F_p(k) = F_T(k) = 1$ , which reduces the cross section greatly. Nevertheless, it is not enough argument for the potential bremsstrahlung. Since the potential is originated from the nucleon-nucleon interaction, the  $\gamma$ -ray energy is released by the nucleon interacting with the other nucleon. Therefore, in order to regard the photon as emitted from whole projectile or target, it is required that the recoil momentum of the nucleon, which emits a photon after (or before) the interaction, should be shared with the remainder nucleons so as to form the ground state of the projectile or the target nuclei. Thus one needs to consider a time extent as well as the spatial one.

Now, we consider the emission of 50 MeV photons by 65 MeV <sup>3</sup>He bombardments. The reaction time  $\tau_R$  to produce a photon of 50 MeV is estimated to be 4 fm/c in accordance

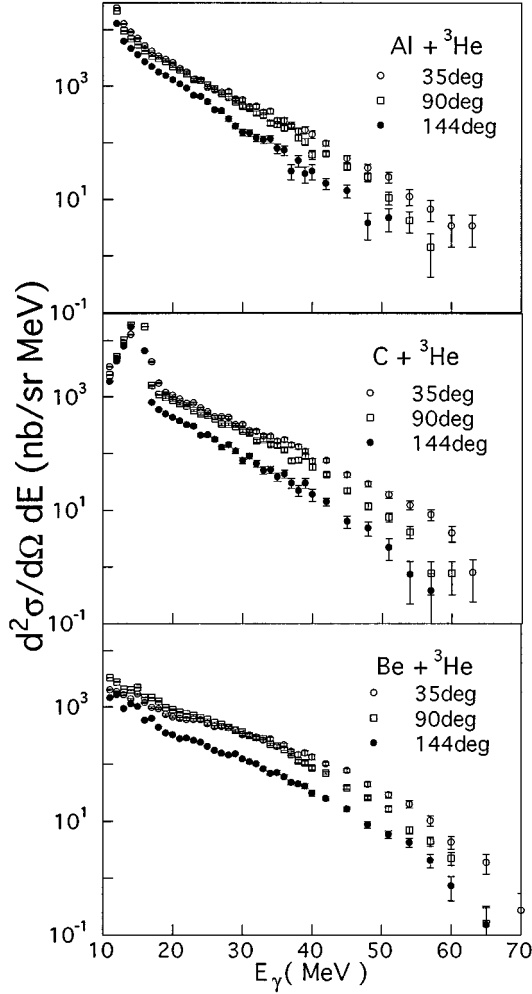


FIG. 5.  $\gamma$ -ray spectra from Be, C, and Al targets bombarded with a 65 MeV  $^3\text{He}$  beam.

with the uncertainty relation. Assuming the interaction range between two nucleons as 1.4 fm, we can consider the emission process where two of the three nucleons sequentially transfer their energies to the remaining one which emits sum of the three nucleon's energies as one photon: the interaction time  $1.4 \times 2 = 2.8 \text{ fm}/c < \tau_R$ . Of course, the crossing time through the surface  $2a/v_p$  should be equal or longer than the reaction time  $\tau_R$  (we assume the length of nuclear surface as  $2a$  and denote the velocity of projectile as  $v_p$ ). On the other hand, a nucleus which consists of more than three nucleons is expected not to produce such a high-energy photon by the reason mentioned above. In the present case, we can therefore neglect the contribution from the target nuclei (Be, C, and Al) to the production of high-energy  $\gamma$  rays. This is the reason that, in high-energy heavy-ion collisions,  $\gamma$  rays near the kinematical maximum energy have not been observed in the experiments up to now. For even higher-energy light-ion collisions ( $E > 100 \text{ MeV}$ ), the  $\gamma$  rays near the kinematical maximum energy are not expected in the potential bremsstrahlung because the reaction time for such high-energy  $\gamma$  rays becomes too short.

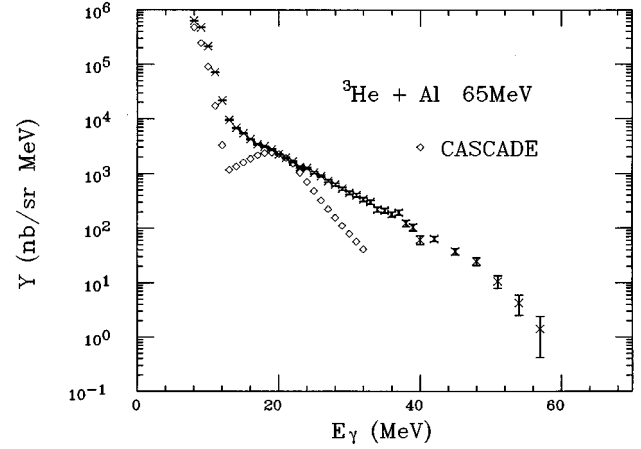


FIG. 6. Comparison with the cascade decay  $\gamma$  rays.

#### IV. DISCUSSION AND CONCLUSION

Three origins can be considered for the production of continuous high-energy  $\gamma$  rays; emitted from a nucleus highly excited through the compound reaction process, the nucleon-nucleon bremsstrahlung, and the potential bremsstrahlung. The contribution of  $\gamma$  rays from the compound nuclei can be estimated by the statistical model calculation. We have performed such calculations by using the code CASCADE [11] with standard parameter values for the level density and the giant dipole resonance. The result of the calculation for the  $^3\text{He} + \text{Al}$  reaction is shown in Fig. 6 with the experimental data. Although the  $\gamma$  rays emitted through the giant resonance make a broad peak structure around 20 MeV,  $\gamma$ -ray yields for  $E_\gamma > 30 \text{ MeV}$  are at least 1 order of magnitude smaller than the experiment. Thus, the contribution of the decay  $\gamma$  rays is negligible.

In the nucleon-nucleon bremsstrahlung model, the emitted  $\gamma$  rays are considered to be created incoherently from each nucleon-nucleon interaction in the mean field during the collision. The emission of  $\gamma$  rays with energies higher than half of the incident energy per nucleon, then, requires the high-momentum component of the Fermi motion of the nucleon in the projectile and target nuclei. The simplest estimation based on the nucleon-nucleon bremsstrahlung is to calculate the first chance nucleon-nucleon collision with the experimental value of the bremsstrahlung cross sections. In this case, however, the energy-momentum conservation of the whole system cannot be incorporated; this requirement is essential especially for the present case where the almost available energy is converted to the single  $\gamma$ -ray emission. Generally, more sophisticated calculations, such as BUU calculations, have been performed using the transport equation with collision term. However the momentum-energy conservation of the whole system is not incorporated in most of the calculations. Therefore, the calculation with the conventional code usually overestimates near the kinematical maximum energy; if the system has enough energy after the  $\gamma$ -ray emission, the calculation is worthy to be compared with the experiment. Knowing these restrictions, we have compared the production cross sections for the  $^3\text{He} + ^{12}\text{C}$  reaction with those calculated by using the BUU code [3]. As shown in

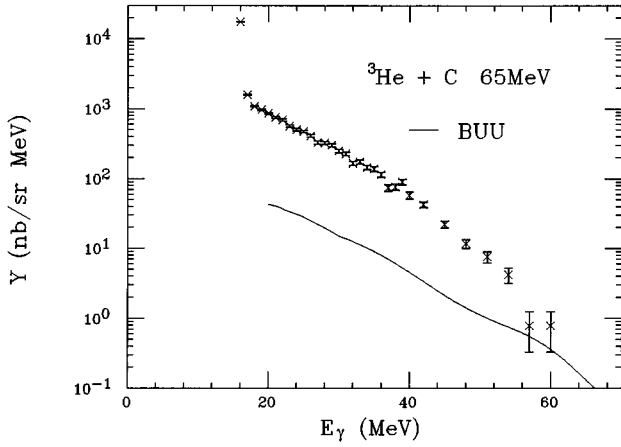


FIG. 7. Comparison with the nucleon-nucleon bremsstrahlung.

Fig. 7, the calculated yields at around  $E_\gamma=40$  MeV are smaller than the experiment. Although the calculated yield at the maximum energy becomes same order of magnitude as the experiment, this is due to the lackness of the momentum-energy conservation as discussed above. Therefore, the contribution of the incoherent nucleon-nucleon bremsstrahlung is at least one order of magnitude smaller than the observed yields for  $E_\gamma>40$  MeV and a large contribution of other bremsstrahlung should be considered in this energy region. Tam *et al.* investigated the bremsstrahlung for the  $^4\text{He}+^{12}\text{C}$  reactions at  $E/A=25$  MeV and  $E/A=53$  MeV and also for the  $^2\text{H}+^{12}\text{C}$  reaction at  $E/A=53$  MeV [12]: the calculation of BUU reproduces both the experimental cross sections of bremsstrahlung for the  $^4\text{He}+^{12}\text{C}$  reaction at  $E/A=53$  MeV and those for the  $^2\text{H}+^{12}\text{C}$  reaction at  $E/A=53$  MeV, and it overestimates for the  $^4\text{He}+^{12}\text{C}$  reaction at  $E/A=25$  MeV.

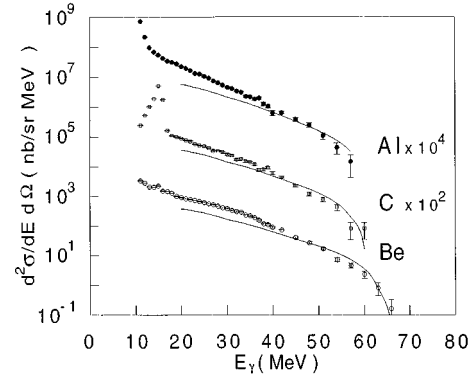


FIG. 8. Energy spectra of the potential bremsstrahlung at  $90^\circ$ .

The present experimental cross sections for the  $^3\text{He}+^{12}\text{C}$  reaction at  $E/A=21.7$  MeV are larger than those of the  $^4\text{He}+^{12}\text{C}$  reaction at  $E/A=25$  MeV, whereas the calculated cross sections of BUU for the former reaction are one order of magnitude smaller than those for the latter reaction. Our results are just contrary to those of Tam *et al.* [12]

Calculating the production cross sections of potential bremsstrahlung in accordance with the last section, transforming them into the laboratory frame, and then convoluting them with the  $\gamma$ -ray energy response function, we obtained cross sections corresponding to the experimental ones. We did not unfold the experimental  $\gamma$ -ray spectra since the  $\gamma$ -ray cross sections at the kinematical maximum energy could not be obtained owing to relatively poor statistics. In order to facilitate comparisons with our experimental  $\gamma$ -ray spectra, we present the response function of our detection system for  $\gamma$  rays of the energy  $E_0$  (in MeV), which is deduced by fitting a Gaussian function jointed to an exponential left-hand tail to the experimental spectra shown in Fig. 3:

$$Y(E, E_0) = \begin{cases} X1 \times \exp[-(E - X2)^2 / X3], & E \geq X2 - \frac{X3 \times X4}{2}, \\ X1 \times \exp[(E - X2)X4 + X3 \times X4^2 / 4] & E \leq X2 - \frac{X3 \times X4}{2}, \end{cases}$$

with

$$X1 = 0.3 - 0.003E_0,$$

$$X2 = -0.51 + 0.97E_0,$$

$$X3 = 1.1 + 0.08E_0,$$

$$X4 = 0.97 - 0.021E_0 + 0.00013E_0^2. \quad (6)$$

The detection efficiency due to the rejection of cosmic muon rays is taken into account in the above equation.

We fitted the theoretical cross sections to the experimental ones, by changing the parameters of  $V_0$  and  $S$ . The geometrical parameter  $a$  was taken as 0.774, 0.784, and 0.805 fm for the targets of Be, C, and Al, respectively, as was deduced by

Trost *et al.* [13] The results on the energy spectrum obtained at  $90^\circ$  are shown in Fig. 8 and those on the angular distribution in Fig. 9, where the solid curves represent the theoretical cross sections for the potential bremsstrahlung. It is seen from these figures that the predictions of the potential bremsstrahlung well reproduce the experimental  $\gamma$ -ray spectrum, especially in the energy region near the kinematical maximum energy. As a result of comparisons with the potential bremsstrahlung, we can recognize another component of continuum  $\gamma$  rays in the spectra of Be, C, and Al, respectively (Fig. 8). This component is expected to be the potential bremsstrahlung of two nucleons in  $^3\text{He}$ , because the maximum energy of this bremsstrahlung is estimated to be approximately 40 MeV in consideration of the beam energy per nucleon. Development of a theory for such potential bremsstrahlung is strongly desirable.

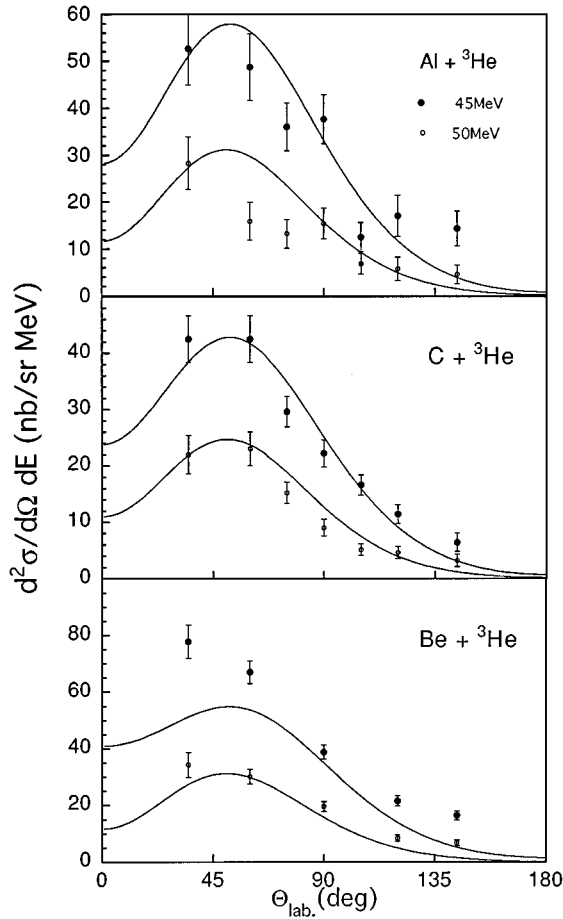


FIG. 9. Angular distributions of the potential bremsstrahlung.

For the potential bremsstrahlung of 50 MeV, the reaction time  $\tau_R$ , the interacting time of nucleons in  ${}^3\text{He}$  nucleus  $\tau_I$ , and the crossing time through the nuclear surface  $\tau_C$  are estimated to be 4, 2.8, and 8 fm/c, respectively, and satisfy

TABLE I. Best-fit values of  $V_0$  and  $S$ .

Target	$V_0$ (MeV) Potential brems.	$V_0$ (MeV) Elastic scatt.	$S$ (MeV)	$Q$ value (MeV)
Be	-275	-105.8	21.0	26.3
C	-275	-105.7	12.1	12.1
Al	-241	-109.8	5.5	17.9

the time relations of  $\tau_R > \tau_I$  and  $\tau_R < \tau_C$  mentioned in the last section. Pinston *et al.* [14] measured high-energy  $\gamma$  rays in the  ${}^3\text{He}$ -induced reactions at 280 MeV. In this case, however, the emission of  $\gamma$  rays of high energy near the kinematical maximum energy cannot be expected, since  $\tau_R$  for 280 MeV  $\gamma$  rays is 1.4 fm/c, i.e.,  $\tau_R < \tau_I$ . Actually such high-energy  $\gamma$ -rays were not observed in their data.

Table I presents the best fit values of  $V_0$  and  $S$ . We also list in this table the experimental values of  $V_0$  deduced from  ${}^3\text{He}$  elastic scattering data by Trost *et al.* [13] and the  $Q$  values [15] corresponding to the difference between the total mass of projectile and target nuclei and the mass of their fused nucleus. The values of  $V_0$  for the potential bremsstrahlung are about 2.5 times larger than those of the elastic scattering. This fact denotes that the projectiles are strongly accelerated in the case of potential bremsstrahlung. The values of  $S$  are smaller than the  $Q$  values. This can be interpreted in such a way that the three nucleons of projectile can exist as  ${}^3\text{He}$  particle in the fused nucleus only with the excitation energies higher than  $Q-S$ . Thus, we conclude that the experimental data in the high-energy region of  $E_\gamma > 40$  MeV can be interpreted as the potential bremsstrahlung.

#### ACKNOWLEDGMENTS

The authors would like to thank T. Honma, S. Kan, K. Ishiwata, S. Chiba, and N. Takahashi for operating the cyclotron throughout the experiment.

- [1] H. Nifenecker and J. A. Pinston, *Prog. Part. Nucl. Phys.* **23**, 271 (1989).
- [2] H. Nifenecker and J. A. Pinston, *Annu. Rev. Nucl. Sci.* **40**, 113 (1990).
- [3] W. Cassing, V. Metag, U. Mosel, and K. Nitta, *Phys. Rep.* **188**, 363 (1990).
- [4] K. Nakayama and G. F. Bertsch, *Phys. Rev. C* **34**, 2190 (1986).
- [5] K. Nakayama and G. F. Bertsch, *Phys. Rev. C* **36**, 1848 (1987).
- [6] K. Snover, *Annu. Rev. Nucl. Sci.* **36**, 545 (1986).
- [7] G. Reffo, M. Blann, and B. A. Remington, *Phys. Rev. C* **38**, 1190 (1988).
- [8] M. Laval, M. Moszynski, R. Allemand, E. Comorche, P. Guinet, R. Odru, and J. Vacher, *Nucl. Instrum. Methods* **206**, 169 (1983).
- [9] T. Murakami, J. Kasagi, H. Tachibanaki, K. Yoshida, Y. Shibata, T. Nakagawa, M. Ogihara, S. M. Lee, T. Kubo, and T. Motobayashi, *Nucl. Instrum. Methods A* **253**, 163 (1986).
- [10] S. Sawada, K. Furutaka, M. Hosaka, T. Murakami, T. K. Murakami, J. Kasagi, K. Ishii, S. Itoh, H. Matsuyama, T. Sasaki, T. Terasawa, T. Suda, and K. Maeda, *Laboratory of Nuclear Science Tohoku University Report* 24, 1991, p. 208.
- [11] F. Puhlhofer, *Nucl. Phys. A* **280** 267 (1977).
- [12] C. L. Tam, J. Stevenson, W. Benenson, J. Clayton, Y. Chen, E. Kashy, A. R. Lampis, D. J. Morrissey, M. Samuel, T. K. Murakami, and J. S. Winfield, *Phys. Rev. C* **38**, 2526 (1988).
- [13] H. Trost, P. Lezoch, and U. Strobusch, *Nucl. Phys.* **A462**, 333 (1987).
- [14] J. A. Pinston, V. Bellini, W. Cassing, S. Drissi, J. Guillot, J. Julien, H. Nifenecker, F. Schussler, and M. L. Sperduto, *Nucl. Phys.* **A536**, 321 (1992).
- [15] K. A. Keller, J. Lange, and H. Münzel, *Q-value and Excitation Function of Nuclear Reactions, Part A Q-Value* (Springer-Verlag, Berlin, 1973).